

This work was written as part of one of the author's official duties as an Employee of the United States Government and is therefore a work of the United States Government. In accordance with 17 U.S.C. 105, no copyright protection is available for such works under U.S. Law.

Public Domain Mark 1.0

<https://creativecommons.org/publicdomain/mark/1.0/>

Access to this work was provided by the University of Maryland, Baltimore County (UMBC) ScholarWorks@UMBC digital repository on the Maryland Shared Open Access (MD-SOAR) platform.

Please provide feedback

Please support the ScholarWorks@UMBC repository by emailing scholarworks-group@umbc.edu and telling us what having access to this work means to you and why it's important to you. Thank you.

Aerosol Properties in Cloudy Environments from Remote Sensing Observations

A Review of the Current State of Knowledge

A. Marshak, A. Ackerman, A. M. da Silva, T. Eck, B. Holben, R. Kahn,
R. Kleidman, K. Knobelspiesse, R. Levy, A. Lyapustin, L. Oreopoulos,
L. Remer, O. Torres, T. Várnai, G. Wen, and J. Yorks

ABSTRACT: Aerosol properties are fundamentally different near clouds than away from clouds. This paper reviews the current state of knowledge of aerosol properties in the near-low-cloud environment and quantitatively compares them with aerosols far from clouds, according to remote sensing observations. It interprets observations of aerosol properties from different sensors using satellite, aircraft, and ground-based observations. The correlation (and anticorrelation) between proximity to cloud and aerosol properties is discussed. Retrieval artifacts in the near-cloud environment are demonstrated and quantified for different sensor attributes and environmental conditions. Finally, the paper describes the possible corrections for near-cloud enhancement in remote sensing retrievals. This study is timely in view of science definition studies for NASA's Aerosol, Cloud, Convection and Precipitation (ACCP) mission, which will also seek to directly link aerosol properties to nearby clouds.

KEYWORDS: Aerosol-cloud interaction; Aerosols; Clouds; Remote sensing

<https://doi.org/10.1175/BAMS-D-20-0225.1>

Corresponding author: A. Marshak, alexander.marshak@nasa.gov

In final form 13 May 2021

©2021 American Meteorological Society

For information regarding reuse of this content and general copyright information, consult the [AMS Copyright Policy](#).

AFFILIATIONS: Marshak, Da Silva, Holben, Kahn, Knobelspiesse, Levy, Lyapustin, Oreopoulos, Torres, and Yorks—NASA Goddard Space Flight Center, Greenbelt, Maryland; Ackerman—NASA Goddard Institute for Space Studies, New York, New York; Eck—NASA Goddard Space Flight Center, and Universities Space Research Association, Greenbelt, Maryland; Kleidman—NASA Goddard Space Flight Center, Greenbelt, and Science Systems and Applications, Lanham, Maryland; Remer and Várnai—NASA Goddard Space Flight Center, Greenbelt, and Joint Center for Earth System Technology, University of Maryland, Baltimore County, Baltimore, Maryland; Wen—NASA Goddard Space Flight Center, Greenbelt, and GESTAR/Morgan State University, Baltimore, Maryland

“[A]erosol measured in the vicinity of clouds is significantly different than it would be were the cloud field ... not present.”—Chapter 7 of IPCC AR5

In the 2017 Decadal Survey (DS17), the global scientific community recognized the critical importance of aerosol–cloud interaction (ACI) in the context of climate forcing, cloud feedbacks, and precipitation processes. The most common connotation of ACI is the one-way interaction of aerosols modifying clouds. However, ACI operates both ways, with clouds also influencing aerosols. Specifically, cloud droplets provide the aqueous environment for precursor gas phase substances to form new particulate matter, and for existing particles to grow. Clouds interact with complex fields of relative humidity (RH), updrafts/downdrafts, and precipitation that affect the physical and optical properties, and concentration of particles that cohabit these environments, contributing to vertical transport and removal processes. Yet, the fact that aerosol properties are fundamentally different close to and away from clouds has not been studied extensively.

We live in a cloudy world. For example, Várnai and Marshak (2011), using *Cloud–Aerosol Lidar and Infrared Pathfinder Satellite Observation (CALIPSO)* observations (Winker et al. 2007), showed that 50% of all 1-km pixels identified as “cloud-free” in Moderate Resolution Imaging Spectroradiometer (MODIS) passive imagery are within 5 km of low clouds (Fig. 1). Furthermore, approximately 20% of all MODIS pixels “fall between the cracks,” deemed too cloudy for retrieval by the aerosol algorithm and not cloudy enough for retrieval by the cloud algorithm. This means that a sizable fraction of pixels are unaccounted for in global estimates of “clear sky” and “cloudy sky” radiative effects from these sensors. This is big! We are not accounting for a significant portion of global aerosol radiative effects, because the aerosols in omitted pixels close to clouds have fundamentally different loading and particle physical and optical properties than those in retrievable pixels far from clouds. Although we understand that aerosol properties are different in cloudy environments and have identified some of the processes responsible

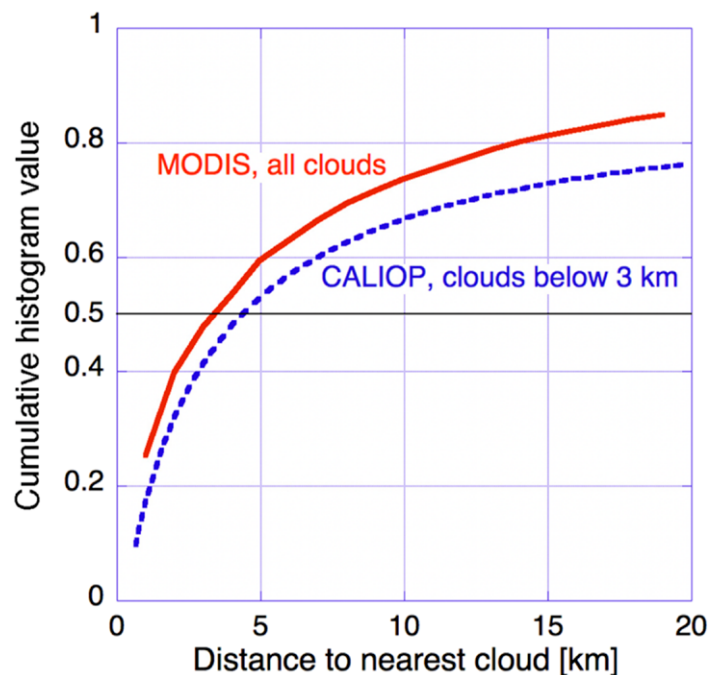


Fig. 1. Cumulative histogram of cloud-free atmospheric columns over all oceans, between 60°N and 60°S latitudes. The solid curve is for all 1-km-size MODIS pixels with viewing zenith angles less than 20° from 21 Jun 2008; the dashed curve is for all 333-m-size columns observed at night by CALIOP between 15 Sep and 14 Oct 2008. The dashed curve is based on the inset in Fig. 1a from Várnai and Marshak (2011) with permission.

for these differences, we do not yet have sufficiently robust algorithms to quantify how these cloud-affected aerosols impact radiation fields and climate forcing.

Initial work on aerosol properties in cloudy environments was purely empirical, mostly using satellite observations that showed a positive correlation between retrieved aerosol optical depth (AOD) and cloud fraction (CF) (Loeb and Manalo-Smith 2005; Zhang et al. 2005). In subsequent, more in-depth work, Charlson et al. (2007) and Koren et al. (2007) urged the field to rethink the traditional clear sky versus cloudy sky parsing of satellite images, leading to works that associated AOD with distance to the nearest cloud (Su et al. 2008; Redemann et al. 2009).

Koren et al. (2007) also examined the putative “cloud-free” region between clouds using MODIS and the ground-based AERONET network data, and showed that in reality this region might not be entirely cloud-free, having reflectance that decreases linearly with logarithmic distance to the nearest cloud with a length scale of ~ 10 km. In a later study, Koren et al. (2009) referred to their 2007 work as being able to identify “the radiative importance of this ‘inter-cloud region’ and the pitfalls of artificially separating ‘direct’ (aerosol only) and ‘indirect’ (cloud) radiative forcing.” In a study using models and remote sensing observations, Charlson et al. (2007) had noted that “current estimates of aerosol climate forcing rely on the conventional expression for albedo ... that ‘direct’ and ‘indirect’ aerosol effects are separately calculated for the clear and cloudy portions of Earth. This approach would be appropriate if the atmosphere consisted entirely of nearly clear and overcast regions The existence of partly cloudy regions and the fact that the clear-cloudy distinction is ambiguous (Fig. 2) and aerosol dependent raise the possibility that the conventional expression may lead to errors.” In addition, Twohy et al. (2009) estimated that the aerosol direct radiative effect in the vicinity of clouds is 35%–65% larger than that from large cloud-free regions whereas Chand et al. (2012) analyzing MODIS data found a 25% enhancement in AOD under cloudy conditions ($CF = 0.8$ – 0.9) compared to relatively clear conditions ($CF = 0.1$ – 0.2).

Given the many questions surrounding aerosol properties in the near-low-cloud environment, we deemed necessary to provide here a review of the current state of knowledge and bring together the relevant information scattered across the literature, sometimes in papers that may have not necessarily had this particular problem as their main focus. In particular, we interpret derived aerosol properties such as AOD and particle size from existing sensors on satellite, aircraft, and ground-based platforms; discuss their correlation with CF; explore the possibility that they are affected by retrieval artifacts in the vicinity of clouds; and quantify them for different sensor attributes and environmental conditions. We also present options for possible correction for near-cloud enhancement and conclude with an assessment of the observational and modeling efforts needed to better understand and define aerosol properties near low clouds. We limit the scope of the current review to nonprecipitating clouds, and consider only remote sensing observations, leaving the important subject of implied impacts on aerosol forcing and cloud feedbacks for other works.

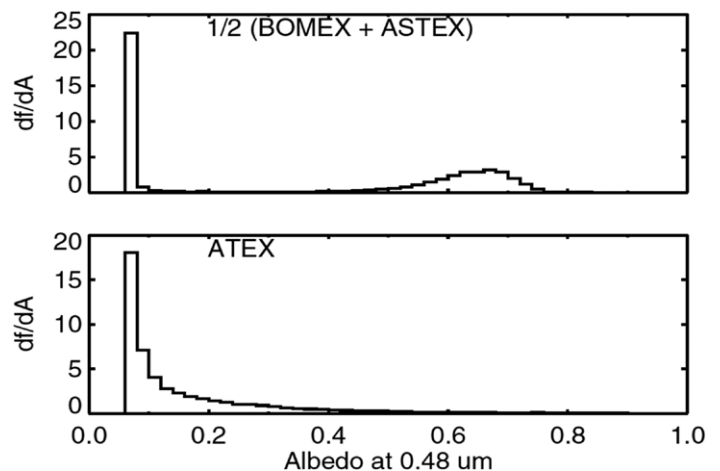


Fig. 2. Inseparability of cloudy and clear skies under partial cloud cover. Plots show albedo pdfs from large-eddy simulations of trade cumulus (Cu) and stratocumulus (Sc) clouds. (top) The average of the BOMEX ($\sim 10\%$ cloud cover) and ASTEX (overcast) fields; clear and cloudy contributions are nicely separated. (bottom) ATEX trade Cu ($\sim 50\%$ cloud cover), with the albedos from clear and cloudy portions inseparable. (From Charlson et al. 2007.)

Aerosol observations near low clouds

Ground-based remote sensing of aerosol–cloud interactions. A series of papers investigating aerosol modification by cloud and fog were published from 2012 to 2020 based on ground-based AERONET remote sensing measurements of AOD and retrievals of column-integrated aerosol size distributions. AERONET almucantar retrievals (Dubovik and King 2000; Dubovik et al. 2006; Holben et al. 1998) at locations with recent significant air pollution episodes exhibited bimodal submicron size aerosol distributions where fog and/or low-altitude stratiform cloud had recently evaporated (Eck et al. 2012). These locations include the Indo-Gangetic Plain in India, the Central Valley of California, the Beijing region in China, South Korea, the coast of Chile, the Po River Valley in Italy, and São Paulo, Brazil. The larger-sized mode of these bimodal fine mode cases was typically $\sim 0.4\text{--}0.5\text{-}\mu\text{m}$ radius peak in volume size distribution, and likely consisted of particles processed by fog and/or cloud droplets. The smaller mode typically at $0.12\text{--}0.20\text{-}\mu\text{m}$ radius may have been interstitial aerosol that was not modified by incorporation in droplets and/or aerosol that was less hygroscopic in nature. The smaller mode may have also been aerosols that were at altitudes above (or below) cloud layers or have been advected to the location of the evaporated clouds, thereby not interacting with clouds. The larger mode particles had weak absorption and were also associated with higher optical depths due to increased scattering efficiency. Li et al. (2014) found these large submicron particles ($0.44\text{-}\mu\text{m}$ modal radius) from almucantar retrievals during the extreme air pollution event in Beijing from 11 to 14 January 2013. Geostationary satellite images showed the presence of fog during this Beijing pollution event that had record high PM_{2.5} concentrations. Similar size large submicron radius particles have been observed from in situ measurements of cloud or fog processed aerosols. Dall’Osto et al. (2009) measured particles of $0.4\text{--}0.5\text{-}\mu\text{m}$ volume radius in a London fog event and identified them as hydroxymethane sulfonate (HMS), which are only formed in aqueous phase chemistry and are therefore tracers of cloud processing of aerosols.

An example of a submicron bimodal size distribution AERONET retrieval with nearby clouds and fog in South Korea is shown in Fig. 3 (Eck et al. 2018). The climatological mean

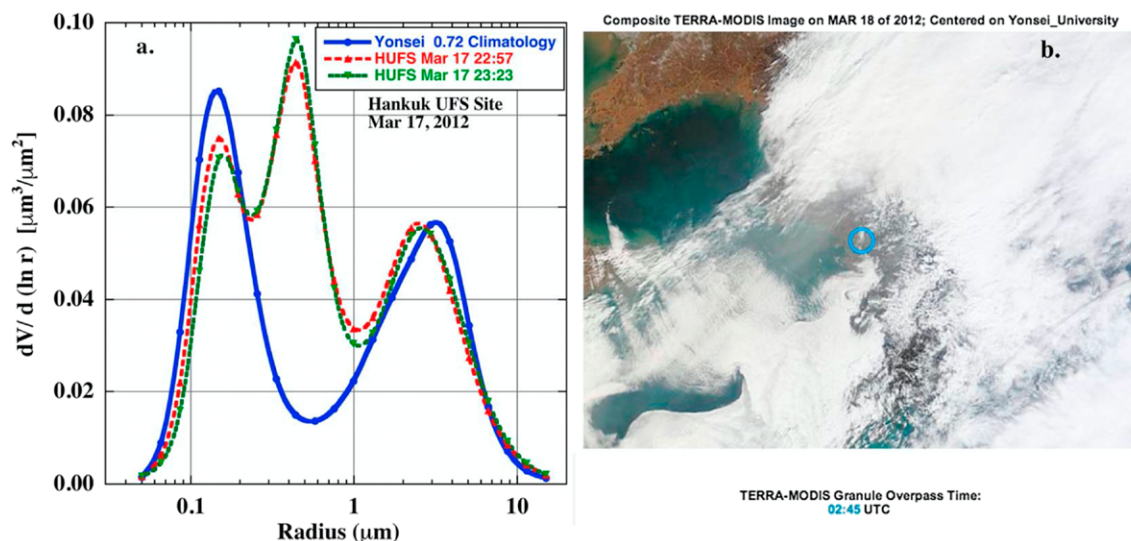


Fig. 3. (a) Almucantar retrievals of aerosol size distributions from AERONET measurements made at the Hankuk UFS (HUFS) site on 17 Mar 2012 (times in UTC), as compared to climatological mean size distributions from the Yonsei University site utilizing 42 retrievals from March to May 2011 and 2012 with average fine mode fraction (440 nm) of 0.88 and AOD (440 nm) ranging from 0.6 to 0.8. (b) MODIS *Terra* image from about 4 h after the Hankuk UFS retrievals shown in (a). The blue circle indicates the Yonsei University site location. Based on Fig. 6 from Eck et al. (2018) with permission.

size distribution is shown for comparison. The middle mode size particles are not present in the climatology and exist only for the cloud/fog processing case such as in this 17 March 2012 example, with particle size similar to HMS as measured by in situ instruments. Although these middle mode events are not common in South Korea, they are significant in terms of air quality. Eck et al. (2020) showed that these fog-processed aerosol cases are associated with high PM_{2.5} measurements in Seoul in May and June 2016, with particulate levels exceeding the national air quality standard. Moch et al. (2018) showed that HMS in Beijing may be a key chemical constituent enabling the formation of particles in cloud droplets thereby contributing to severe air pollution events. Furthermore Ma et al. (2020) measured high concentrations of HMS in Beijing during winter haze events and associated the formation of HMS in aerosol water at high RH levels. The very large size accumulation particles were not seen in AERONET observations in any cases of aerosol retrievals under polluted conditions when low cloud or fog was not present. Since aerosol optical depth was observed to increase as fine radius increased in such cases, the sampling bias of cloud-processed aerosols in the near-cloud environment likely results in an *underestimation of total AOD* from most satellite and ground based remote sensing observations, and therefore an *underestimation of aerosol direct radiative effect* in this type of environment. This also holds true for aerosols enlarged by hygroscopic growth in the near-cloud high RH environment.

A very different type of aerosol modification by clouds was observed from AERONET measurements of AOD in the near vicinity of nonprecipitating cumulus clouds in Maryland, United States (Eck et al. 2014), during the DISCOVER-AQ large-scale field campaign. Rapid increases in AOD at 500 nm, at rates of up to 75% in 13 min, were observed by direct sun measurements following cumulus cloud development during July 2011 (Fig. 4). During this time period of rapid AOD increase, the Ångström exponent (AE) remained relatively constant throughout the day. This suggests that the increase in AOD was not exclusively due to humidification-driven particle growth since in that case the short wavelength (380–500 nm) AE would have decreased from pre- to postcumulus occurrence. Therefore, *the extinction of humidified and swelled particles was likely offset by smaller newly formed particles* due to gas-to-particle conversion in cloud droplets that subsequently evaporated. Figure 5 in Eck et al. (2014) shows a MODIS Aqua afternoon image on this same day (5 July 2011) along with time series plots of

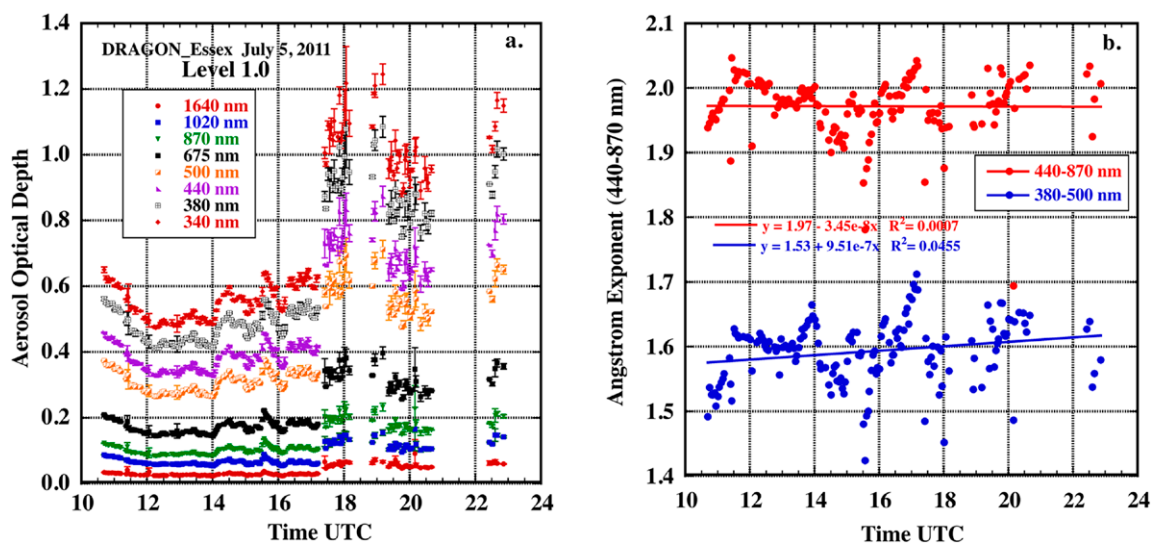


Fig. 4. (a) The time series of spectral AOD measured at the DRAGON_Essex AERONET site on 5 Jul 2011, for data with no cloud screening (level 1.0). The bars shown are \pm half of the AOD triplet range (maximum–minimum AOD). (b) The time series of the Ångström exponent computed for two wavelength intervals from the same data as in (a), including the linear fit to both. Based on Fig. 3 in Eck et al. (2014) with permission.

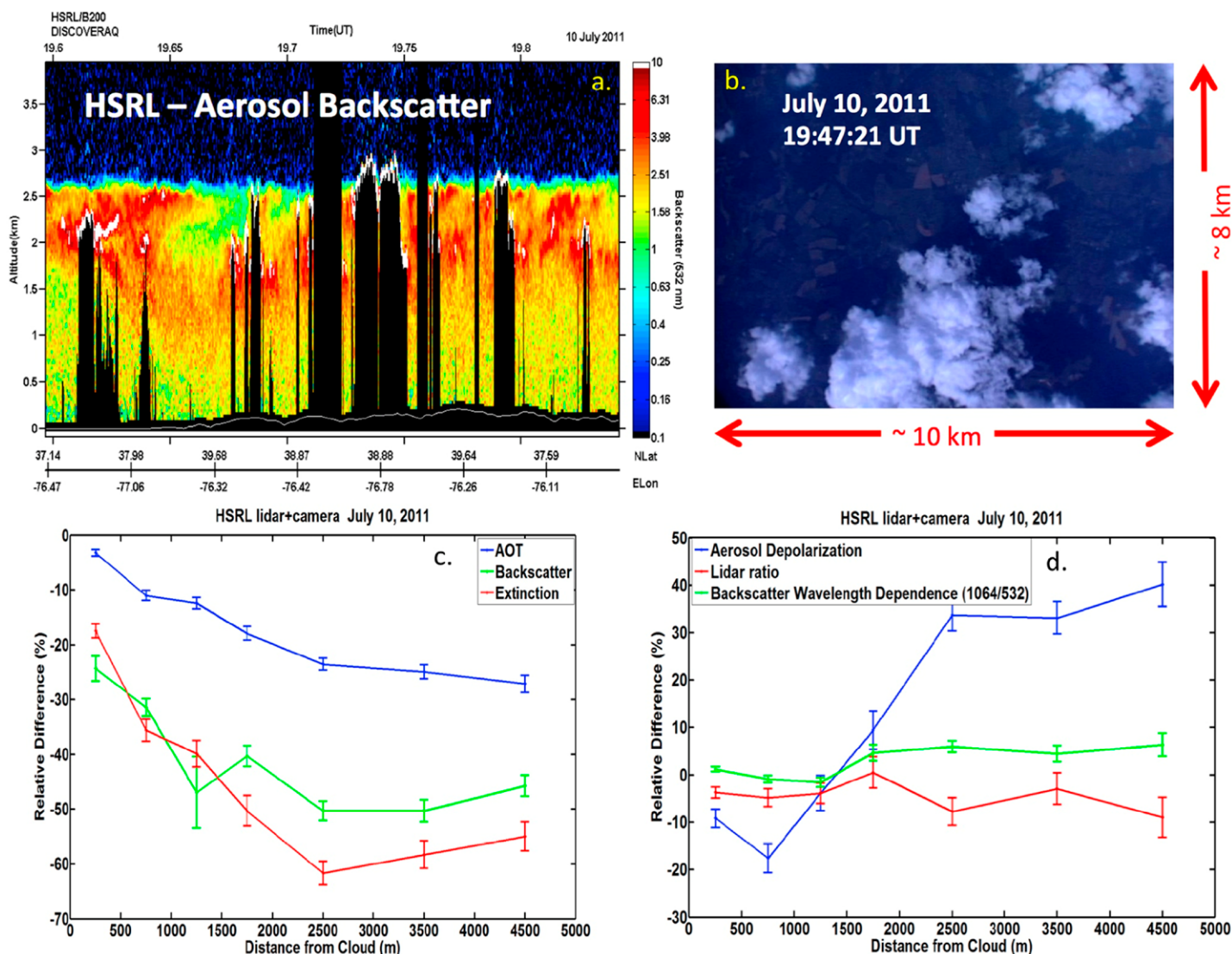


Fig. 5. (a) Downward viewing HSRL measured backscattering coefficient (532 nm) from a 15-min flight segment corresponding to a ~90-km transect on 10 Jul 2011 in the Maryland study region. (b) An example digital camera image taken coincident with the HSRL data in order to determine the distance from cloud of each lidar scan pulse. (c) Aerosol extensive parameters (backscatter, extinction, and AOD) inferred from HSRL data as a function of distance from the cloud edge. (d) Aerosol intensive parameters (depolarization, lidar ratio, and backscatter wavelength dependence) inferred from the HSRL data as a function of distance from the cloud edge. From Fig. 10 in Eck et al. (2014) with permission.

AOD for nine different AERONET sites within the scene. Sites that were close to the larger cumulus clouds on 5 July 2011 afternoon exhibited large increases in fine mode AOD after cloud formation (morning was nearly cloudless) while sites near small cumulus clouds or relatively cloudless showed stable or relatively flat time series in AOD. Some sites showed even larger increases in AOD associated with cumulus development than at the DRAGON_Essex shown in Fig. 4. Additionally, a similar case 5 days later on 10 July 2011 in central Maryland had a greater than 300% increase in AOD (over ~2 h) at a site in the same region, again associated with cumulus development in the afternoon with nearly cloudless morning. Furthermore, other coincident measurements from independent platforms and instrument types (lidar and in situ from aircraft) on this date confirmed that these AOD enhancements were associated with the proximity to cumulus clouds and not related to other meteorological factors. Airborne High Spectral Resolution Lidar (HSRL) measurements measured rapid AOD increases in the vicinity of cumulus clouds but no gradient in lidar color ratio (1064/532 nm) as a function

of distance from cloud suggesting no change in particle size near clouds, while showing an average ~20%–25% increase in AOD from a 4.5-km distance to cloud edge (Fig. 5). Note that these values are averages including both small and large clouds, whereas the much larger AOD increases in AERONET measurements occurred adjacent to the largest clouds. Airborne in situ particle measurements on the same day at ~1–1.5-km altitude showed the aerosol number concentration increasing by ~50% from pre- to postcumulus formation. However, flights at altitudes above 1.3 km indicated that the mean geometric diameter shifted to ~50% larger sizes after cloud formation. These results suggest two different processes occurring simultaneously depending on relative location to cumulus clouds: 1) aerosol particle formation and/or redistribution below the cloud base leading to an increase in aerosol concentration and 2) cloud processing and/or humidification of existing aerosols above the cloud base leading to an increase in aerosol size.

Arola et al. (2017) conducted a study of the entire global AERONET database (version 2) to assess the fine mode AOD in near cloud environments using a spectral deconvolution algorithm (SDA) that separates fine and coarse mode components, and which therefore can observe fine mode AOD even in partially cloud contaminated observations since it assigns cloud droplets to the coarse mode. When the cloud-screened fine mode AOD for June–August was compared to its non-cloud-screened counterpart a global 0.011 AOD enhancement, corresponding to an average increase of 7% over all AERONET sites, was found in cloudy environments. The cloudy sky AOD enhancements were greatest in Asia with a 10% relative increase in fine mode AOD, with some sites in the Beijing, China, region having seasonal enhancements in fine mode AOD that reached 0.10. The largest enhancements in cloudy conditions occurred both globally and regionally during June–August. These large enhancements in northeastern Asia are consistent with the analysis of Eck et al. (2018), who found that the AERONET cloud screening eliminated many high fine mode AOD days with AOD at 500 nm > 1 near Beijing and in Seoul. Arola et al. (2017) also found that the AE decreased slightly when the fine mode AOD increased in the cloud enhanced data. However, the measured AE decreases typically averaged 0.02 or less, therefore suggesting nearly constant fine mode particle size in clear sky versus cloudy environments. This is similar to what was observed in the vicinity of cumulus clouds in Maryland by Eck et al. (2014) where AE remained relatively constant in the near cloud environment despite the near doubling of AOD (Fig. 4), possibly due to the *offsetting effects between new particle formation in clouds* (gas-to-particle chemistry is rapid in cloud droplets) *and the particle growth from both humidification and cloud processing*.

During the 2016 Korea–U.S. Air Quality (KORUS-AQ) campaign and continuing through the entire month of June, Eck et al. (2020) found that the days with the highest values of both AOD and PM_{2.5} were associated with either high cloud amount and/or fog over the Yellow Sea adjacent to the coast of northern South Korea (Fig. 6). These days also suffered pollution transport from China and were sometimes associated with weak cold frontal passage and associated clouds. AERONET retrieved very large fine mode particle sizes during these days where high AOD coincided with clouds and/or fog, suggesting hygroscopic growth in high humidity conditions and possible cloud processing of particles in the fog or clouds. Measurements of AOD enhancement, defined as the ratio of AOD at ambient RH to dried AOD, by in situ instruments from aircraft indicated significant enhancements (~1.7–2) on these days of pollution transport and cloud/fog presence, consistent with humidification-induced large fine mode particle radii retrieved by AERONET. Comparison between the time series of hourly PM_{2.5} data in central Seoul and values near the coast west of Seoul showed that the largest differences in ground level PM_{2.5} between coastal sites and central Seoul during the KORUS-AQ campaign occurred during transboundary pollution transport days. This suggests possible additional aerosol formation from cloud droplets processing urban region gaseous emissions and/or possible additional pH-dependent aerosol formation in aerosol water.

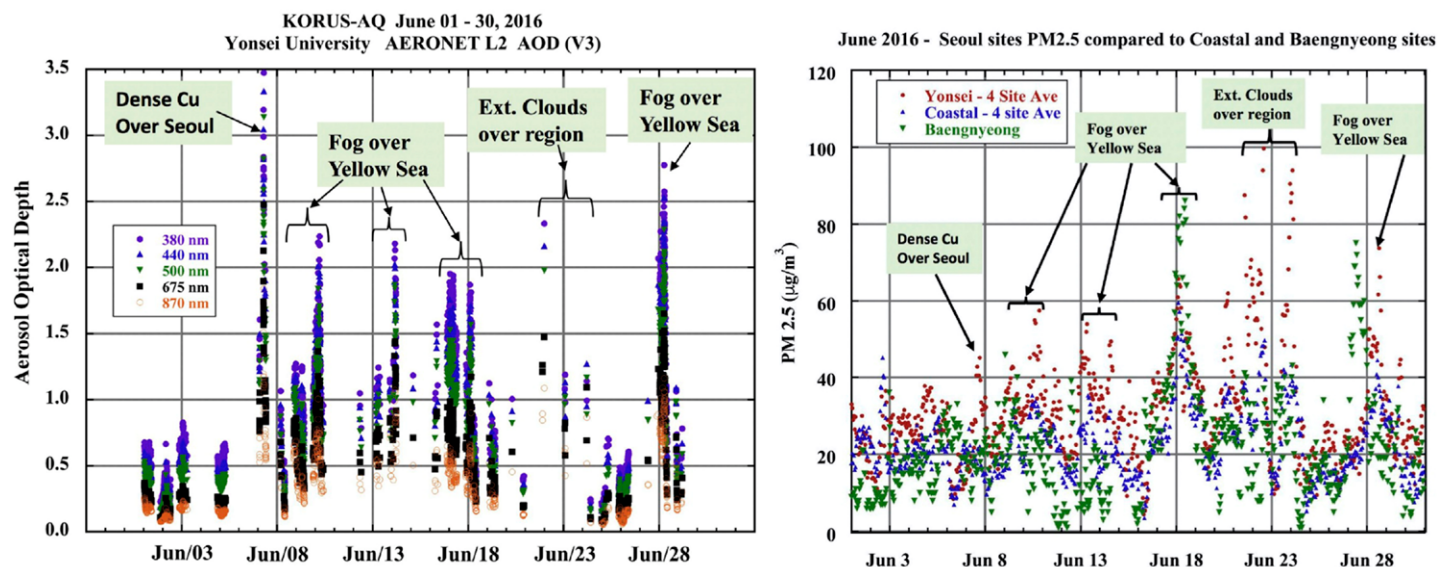


Fig. 6. (left) Time series of AERONET measured spectral AOD at the Yonsei University site for the entire month of June 2016. The date marker indicates the beginning of each day. As noted by the brackets and arrows, all dates when AOD at 500 nm exceeded 1.0 also showed clouds in the vicinity of the site and/or fog over the Yellow Sea to the west of Seoul. (right) Time series of hourly PM_{2.5} measurements for 1–30 Jun 2016 with the Baengnyeong site (~210 km northwest of central Seoul) compared to measurements in central Seoul and the Yellow Sea coast. Note the much higher values in Seoul vs the coastal region for some of the days with highest PM_{2.5} levels, especially 22–23 Jun and 28 Jun. Figures are based on Figs. 7 and 9a (respectively) from Eck et al. (2020) with permission.

It should be noted that above observations of cloud modified aerosols by AERONET were not common and were only detected in specific conditions and/or certain regions. However, remote sensing observations including those from the ground are expected to typically miss many cases of the effects of clouds on aerosols due to clouds blocking direct sun and/or sky radiance measurements.

Aircraft remote sensing of aerosols near clouds. Many studies of aerosols in cloudy environments are based on moderate-resolution passive space-based imagers, such as MODIS and VIIRS. These imagers have native spatial resolution on the order of 0.5–1.0 km (at nadir, depending on band and sensor). Some of the associated aerosol retrieval algorithms, such as the dark-target (DT) algorithm (Levy et al. 2013), work with aggregates of these pixels and provide products at resolutions on the order of 5–10 km. As part of the retrieval process, a statistical filtering of the native-resolution cloud pixels provides a “mask” of pixels that appear to be clouds and/or cloud edges, with the remaining pixels being considered cloud-free observations and used in the aerosol retrieval. However, even after such cloud masking, retrieved AOD tends to be higher near clouds (Marshak et al. 2008; Várnai and Marshak 2009), owing possibly to (i) aerosol “swelling” due to hygroscopic growth near cloud boundaries, (ii) known 3D effects on the satellite-observed radiation following interactions with clouds and the surface, (iii) uncertainties in cloud masking (decision-making cascade), and (iv) uncertainties in the sensor’s response to adjacency effects. The first effect is a physical process and the second effect is due to interpretation of a complex signal by a simplistic model, while the third and fourth effects are due to imperfections of the algorithm and of our knowledge of instrument behavior. Várnai and Marshak (2012) discussed how all these factors affect moderate resolution aerosol products from MODIS.

How do these effects act at much higher spatial resolution? Spencer et al. (2019) explored this question by applying the MODIS DT aerosol retrieval algorithm on observations by the enhanced-MODIS Airborne simulator (eMAS) on the ER-2 aircraft flying at ~20-km altitude

during the 2013 Studies of Emissions, Atmospheric Composition, Clouds, and Climate Coupling by Regional Surveys (SEAC4RS) Airborne Science Campaign (Fig. 7). While eMAS and MODIS observe at similar wavelengths, eMAS provides much better ~50-m native pixel resolution from the ER-2 altitude. Applying the DT algorithm's pixel aggregation strategy, Spencer et al. (2019) retrieved aerosol properties at a resolution of ~0.5 km, a 20× improvement upon MODIS. The authors noted that the eMAS retrieved AOD was higher near clouds, and with a relative enhancement that was even greater than that for MODIS. Following Várnai and Marshak (2012), Spencer et al. (2019) quantified the enhancement by comparing the eMAS-DT retrievals with data from other sources, specifically MODIS, AERONET, and the Cloud Physics Lidar (CPL), also on the ER-2 aircraft.

Figure 7 shows an example of full resolution eMAS, eMAS degraded to MODIS resolution, and associated CPL products from a Studies of Emissions and Atmospheric Composition, Clouds and Climate Coupling by Regional Surveys (SEAC4RS) scene over Kentucky. The study found that (i) AOD is significantly larger in partly cloudy scenes than clear scenes; (ii) compared to the high-resolution product, the lower-resolution product experiences less enhancement due to averaging both close to and far from clouds; (iii) clouds were generally identified correctly according to CPL (high-resolution eMAS retrievals were not seriously cloud contaminated); and (iv) AOD was indeed higher near clouds as indicated by the correlation between CPL and eMAS, but with enhancement much greater for the latter rather than former. This suggests that the enhancement detected by CPL was due to aerosol swelling, and the greater enhancement observed by the eMAS due to 3D effects largely caused by cloud field.

Satellite observations of aerosols near clouds.

DIFFERENCE IN THE AEROSOL PROPERTIES IN THE VICINITY OF CLOUDS FROM MODIS AND CALIPSO.

One of the primary reasons for studying near-cloud aerosols is that a large number of cloud-free atmospheric columns are surrounded by clouds. Figure 1 shows that according to MODIS over oceans the nearest cloud is within 3 km for half of all clear columns, whereas CALIOP

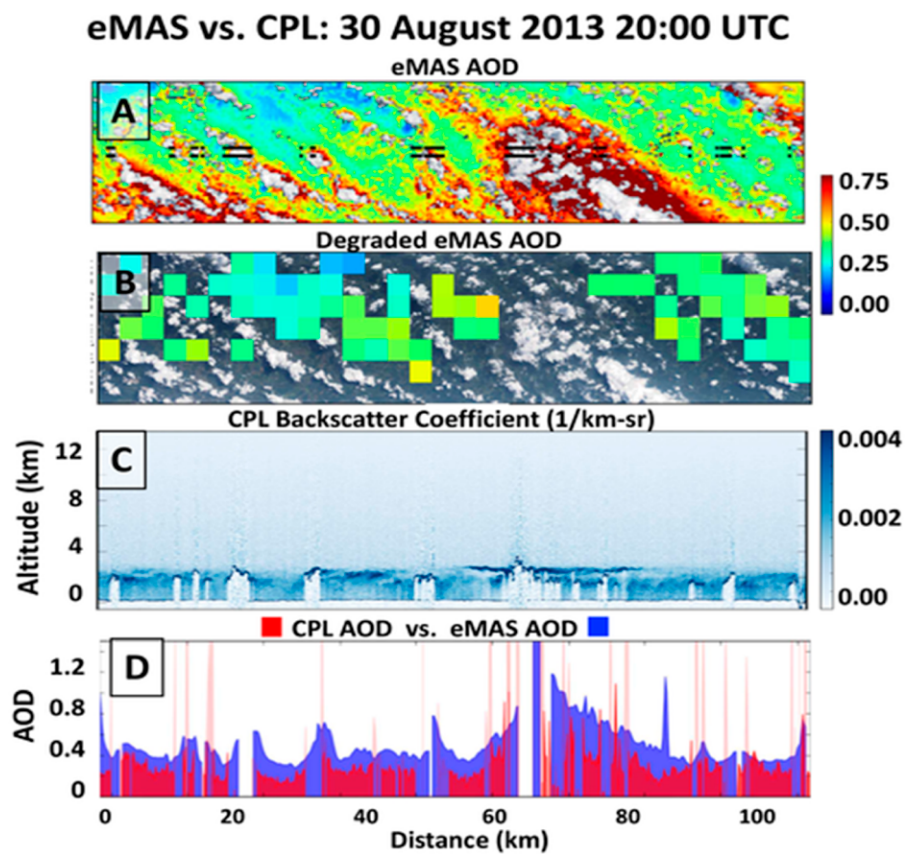


Fig. 7. Airborne remote sensing (from 20-km altitude) of aerosol properties at 2000 UTC 30 Aug 2013 (flight 13959, track 10) over Kentucky, United States. (a) The eMAS retrieved AOD ($0.55 \mu\text{m}$) at 0.5-km resolution superimposed onto a “true-color” RGB image. The black dashes indicate “clouds” detected by the CPL along the center of the eMAS 37-km-wide swath. (b) As in (a), but the AOD retrieval at a degraded 5-km spatial resolution. (c) CPL attenuated total backscatter ($0.53 \mu\text{m}$) profile at 200-m along-track resolution. (d) Comparison of AOD along the center track retrieved from eMAS (at $0.55 \mu\text{m}$ and 0.5-km resolution: in blue) and CPL (at $0.53 \mu\text{m}$ and 200 m: in red). Based on Fig. 16 from Spencer et al. (2019) with permission.

data indicate the nearest low-altitude (below 3 km) cloud is within 4 km. Figure 8 shows that clear sky reflectances systematically increase near clouds regardless of wavelength, as previously shown by Koren et al. (2007). But the rate at which the reflectance increases depends on wavelength which suggests that aerosol populations are systematically different close to clouds.

To better understand the origins of the observed near-cloud radiative changes seen in Fig. 8, we examine how CALIOP lidar returns vary near clouds in Fig. 9. Figure 9a shows that lidar backscatter drops dramatically above the tops of nearby clouds. This happens for two reasons. First, convective clouds tend to reach the top of the boundary layer, and so cloud tops mark the upper limit of the region into which convection (or more generally turbulence) can bring particles from the aerosol-rich near-surface air. Second, undetected cloud particles that increase attenuated backscatter also occur below cloud tops. Additionally, Fig. 9 also reveals that near-cloud increases in both

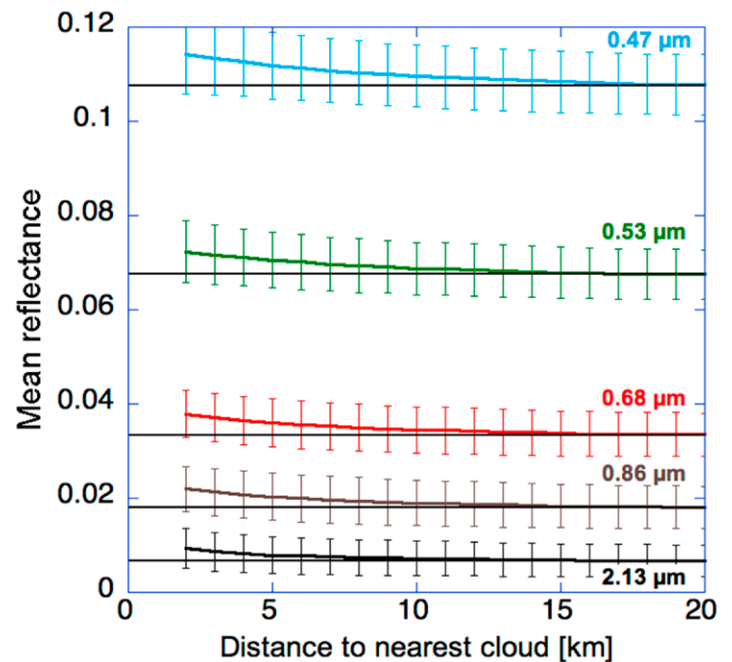


Fig. 8. Average MODIS clear-sky reflectances over a region of the northeast Atlantic Ocean. The horizontal lines indicate mean clear-sky reflectances 20 km away from clouds at various wavelengths. The error bars indicate the standard deviation of near-nadir observations taken between 14 and 29 Sep in each year of the 2000–09 period. The figure is based on Fig. 1a from Várnai and Marshak (2009) with permission.

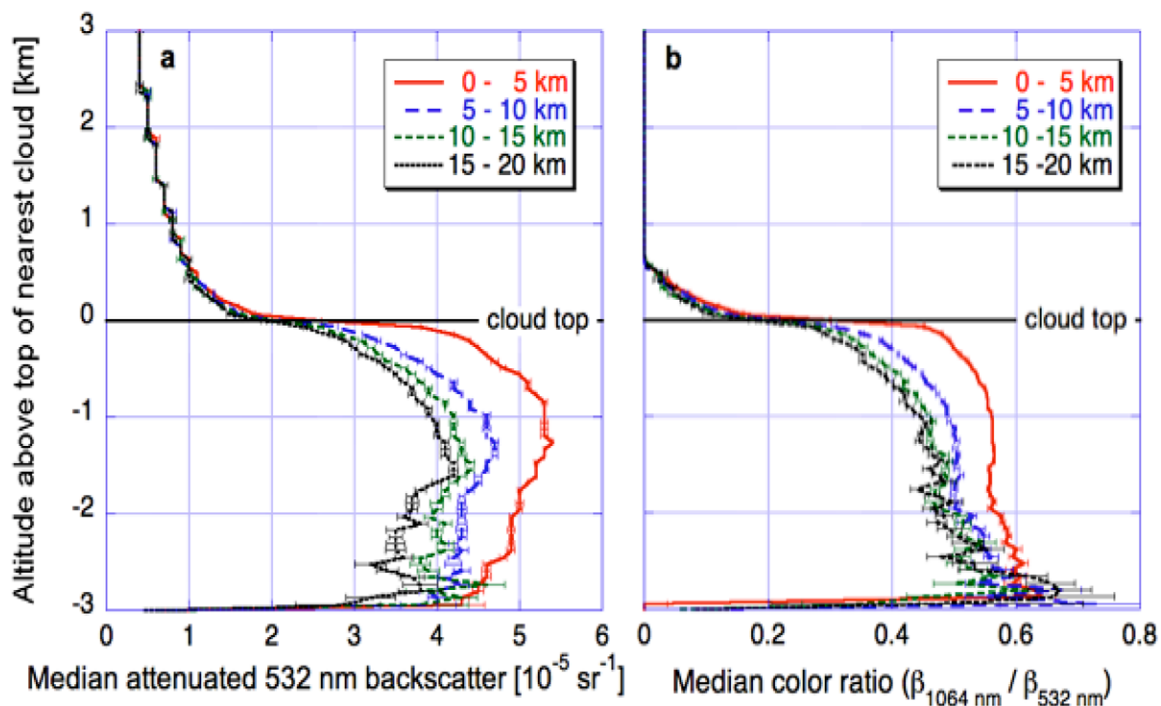


Fig. 9. (a) Median 532-nm attenuated backscatter in different distance ranges from the nearest cloud, plotted as a function of altitude above the top of the nearest cloud. (b) As in (a), but showing median color ratio values (which are related to particle size). Both panels are based on a global dataset of oceanic clear-sky columns where the nearest cloud is below 3 km. The figure is based on Fig. 3 from Várnai and Marshak (2011) with permission.

lidar backscatter (i.e., particle concentration, Fig. 9a) and color ratio (i.e., larger particle size, Fig. 9b) occur below cloud top. We note that this behavior is consistent with CALIOP observations of Saharan dust over the Atlantic Ocean (Yang et al. 2012) showing near-cloud increases in backscatter, color ratio, and depolarization (the latter corresponding to more spherical particles that have swelled in the humid air near clouds) only at the lowest 2 km of the atmosphere (containing most boundary layer clouds).

MISR CONTRIBUTIONS TO UNDERSTANDING AEROSOL PROPERTIES IN CLOUDY ENVIRONMENTS. Multiangle, multispectral imaging from the Multi-Angle Imaging Spectroradiometer (MISR) instrument, orbiting aboard the NASA Earth Observing System's *Terra* satellite, offers two unique capabilities that contribute to understanding aerosol properties in cloudy environments. From MISR hyperstereo, plume height and the associated wind vectors can be derived geometrically (Nelson et al. 2013). This makes it possible to constrain the vertical as well as the horizontal relationships between aerosol plumes and clouds. MISR plume-height retrievals are obtained primarily near major aerosol sources such as wildfires and erupting volcanoes, where plumes are sufficiently optically thick to make aerosol features visible in the multiangle imagery.

In addition, qualitative constraints on particle microphysical properties – size, shape, and light-absorption, can be retrieved radiometrically (Kahn and Gaitley 2015; Limbacher and Kahn 2019). About 3–5 bins in particle size (e.g., “small,” “medium,” and “large”), 2–4 bins in single-scattering albedo (SSA), “flat” or “steep” light-absorption spectral slope, and spherical versus randomly oriented nonspherical particles can be distinguished under good but not necessarily ideal retrieval conditions. To obtain high-quality retrievals, mid-visible AOD of at least ~ 0.15 or 0.2 is generally required. As such, major aerosol plumes provide some of the best MISR particle property retrieval opportunities. Often, the evolution of particles can be inferred from downwind changes in plume-particle properties, and the mechanisms involved, such as size-selective or size-independent gravitational settling, particle hydration, and secondary particle formation, can be inferred. From MISR-observed distances and motion vectors, the spatial and to some extent the temporal scales of the processes affecting particle evolution in the vicinity of clouds can also be deduced.

The eruption of Iceland's Holuhraun volcano between September 2014 and March 2015 offers an example. The aerosol plume created by this volcano was dominated by sulfate particles. MISR imaged the Holuhraun plume 11 times during the first two months of the eruption, after which ambient light levels were too low to obtain satisfactory retrievals (Flower and Kahn 2020). Figure 10, from Flower and Kahn (2020), illustrates the spatial variation of MISR-retrieved *particle effective size, which increases systematically as plume particles approach cloud*. It cannot be determined from these data alone whether plume particles were activated to form the cloud droplets in this case. However, MISR stereo analysis indicates the plume and downwind cloud are at roughly the same elevation, so interaction seems likely. Further analysis, e.g., with coincident MODIS cloud product, might yield additional insights into the relationship between aerosol properties and the ambient meteorological cloud in this case.

OBSERVATIONS OF AOD AND COLUMN WATER VAPOR AT HIGH SPATIAL RESOLUTION. Developing understanding of the aerosol–cloud interactions taking place at small-to-moderate spatial scales ~ 10 – 20 km requires measurements at high spatial resolution. The Multi-Angle Implementation of Atmospheric Correction (MAIAC) is the only operational MODIS algorithm currently making aerosol retrievals at uniform 1-km resolution on a Sinusoidal grid (Lyapustin et al. 2018). MAIAC also produces collocated column water vapor (CWV) with accuracy within $\sim 10\%$ – 15% (e.g., Martins et al. 2019). As RH is the major mediating factor in the transition between aerosol particles and cloud droplets, the availability of combined AOD–CWV retrievals from MAIAC offers rather unique opportunities to study the effects of interest.

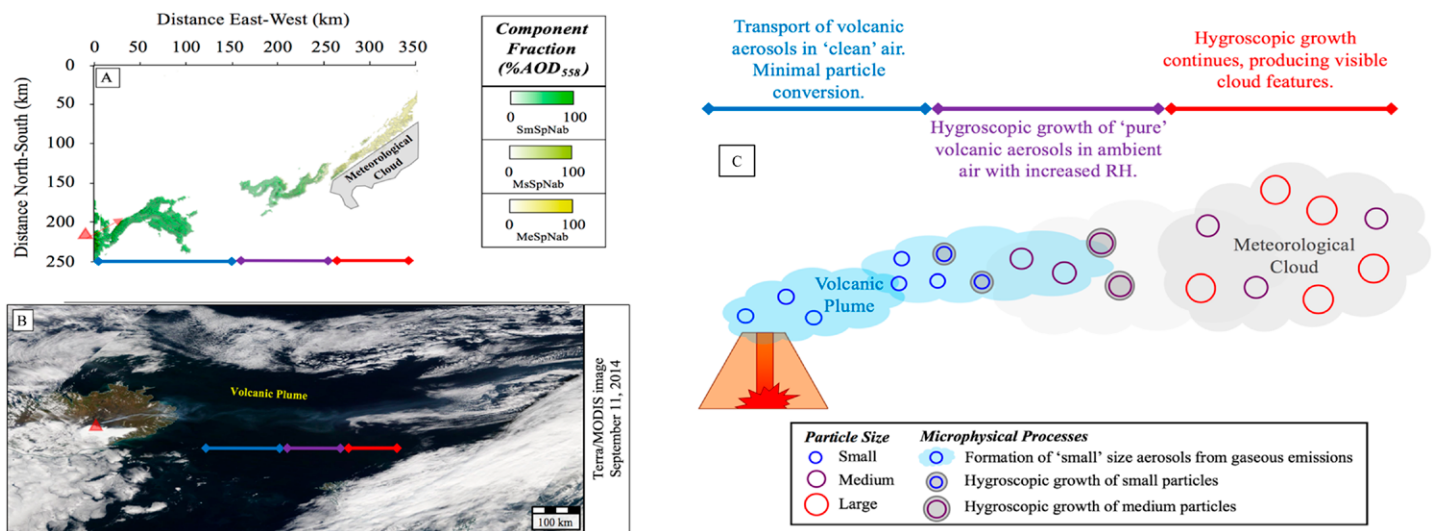


Fig. 10. MISR-retrieved particle properties for the Holuhraun eruption plume of 11 Sep 2014. (a) Map showing the 2D distribution of qualitative particle size, shape, and light-absorption properties retrieved for this event from MISR. Particle types are labeled as: small (Sm), medium–small (Ms), or medium (Me), along with Spherical (Sp) and non-light-absorbing (Nab). Gray color represents meteorological cloud. (b) MODIS true-color context image. (c) Schematic representation of plume evolution based on MISR-retrieved properties. In all three panels, colored arrows highlight the relationship between the volcano, the meteorological cloud, and the segments of the plume. In (a) and (b), red triangles indicate the location of the volcano. The figure is reproduced from Flower and Kahn (2020) with permission.

Figure 11 illustrates a prominent correlated increase of AOD and CWV toward the edge of a cloud. This particular example comes from MODIS *Aqua* measurements acquired on 31 July 2011 over the mid-Atlantic United States. Typically, such a pattern is observed near large cloud systems. It may be associated with aerosol swelling in the updraft zone, or cloud dissipation leaving the field of enhanced AOD and CWV. Occasionally, the latter can be captured by the consecutive MODIS observations from *Terra* and *Aqua* platforms in the course of three hours. Presently, the operational MAIAC algorithm does not provide independently derived spectral AOD information or an effective particle size to characterize effects of cloud processing over land. However, understanding dynamics of these processes helps us draw conclusions about vertical features. For instance, the aerosol particle concentration peaks at or above the cloud bottom height in the case of evaporating clouds. This has implications for air quality analysis as otherwise the enhanced AOD would be associated with the increase of the breathable particulate matter (PM_{2.5}). The dynamics of evaporating clouds along with aerosol enhancement

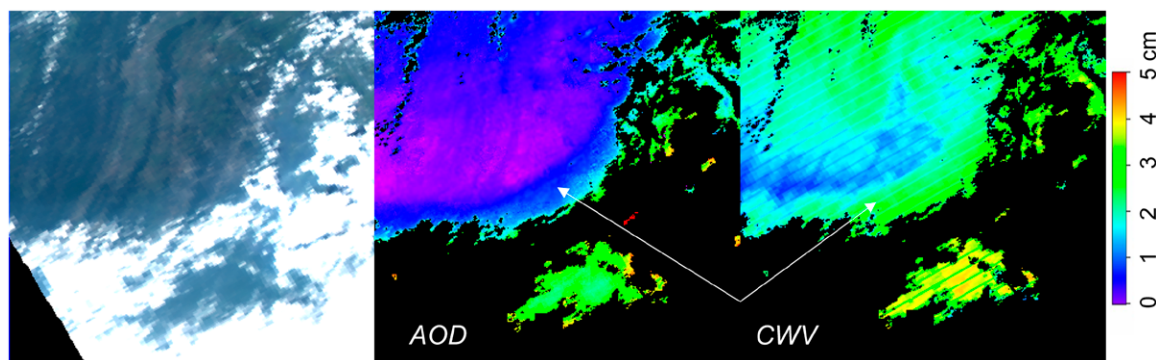


Fig. 11. Illustration of correlated enhancement of AOD at $0.47 \mu\text{m}$ and CWV near large cloud system using 1-km MAIAC data. The image is acquired by MODIS *Aqua* on 31 Jul 2011 over the mid-Atlantic United States. The AOD has the range 0–1 and shares the rainbow palette with the CWV image. The size of the image is 600 km.

from cloud processing can potentially be traced with geostationary observations, e.g., from the Advanced Baseline Imager family of sensors. Unfortunately, these sensors lack the NIR water vapor channel at $0.94\ \mu\text{m}$, preventing us from simultaneously tracking column water vapor at high resolution over land which is possible with MODIS.

NEAR-CLOUD AEROSOL FROM MULTIANGLE POLARIMETERS. Another category of passive remote sensing instruments is capable of measuring at both multiple angles and (linear) polarization states of light. These multiangle polarimeters (MAPs) are intended to maximize observational information content and to provide more extensive and accurate retrievals of geophysical properties (e.g., Mishchenko et al. 2004). Both measurements from existing MAPs (e.g., Parol et al. 2004; Hasekamp et al. 2011; Tanré et al. 2011) and theoretical studies for upcoming instruments (e.g., Hasekamp and Landgraf 2005; Knobelspiesse et al. 2012; Li et al. 2018; Hasekamp et al. 2019a; Remer et al. 2019) show that these instruments are especially skillful in the remote sensing of clouds and aerosols. Here we examine how they can help untangle cloud and aerosol signals in mixed environments.

The greater retrieval fidelity of MAPs can be useful for separating retrieval artifacts in the vicinity of clouds from real aerosol optical property changes, such as refractive index changes due to water uptake. For example, Hasekamp et al. (2019b) created an aerosol cloud condensation nuclei (CCN) proxy from PARASOL observations of aerosol number concentration, size distribution, and particle shape, which was shown to be a more robust proxy of CCN than commonly used aerosol optical depth or aerosol index.

Like other passive remote sensing techniques, radiative transfer calculations needed for the retrieval algorithms of MAPs are performed in one-dimensional (plane parallel) configurations, meaning the 3D effects near clouds can introduce retrieval artifacts. While still relevant, this is less important for MAPs, since multiple scattering tends to weaken polarization (Cornet et al. 2010; Stap et al. 2015, 2016), therefore reducing the impact of 3D effects.

MAPs have unique capabilities for the remote sensing of aerosols and clouds coexisting in the same pixel, specifically if those aerosols are lofted above clouds. From a radiative forcing perspective, the presence of aerosols above clouds can change the apparent albedo and create indirect effects on the cloud properties as well (Yu and Zhang 2013; Knobelspiesse et al. 2015). Recently, several algorithms have been developed to determine aerosol properties above clouds from passive single view angle instruments (Jethva et al. 2013, 2014; Meyer et al. 2015; Sayer et al. 2016). However, these algorithms cannot uniquely determine aerosol loading and absorption, and must make a priori assumptions about the latter. MAPs, however, can independently determine the aerosol and (liquid) cloud state within a single pixel.

Aerosols can independently modify the polarized reflectance away from the cloud bows, so multispectral observations at those geometries can be used to determine both aerosol optical depth and absorption. Thus far, this has been used with the POLDER instrument (Waquet et al. 2009, 2013; Peers et al. 2015) within “super-pixels,” and for a variety of airborne instruments as well (Knobelspiesse et al. 2011; Xu et al. 2018). As in the case for aerosol remote sensing, the computational burden may limit practical large-scale implementation of these retrieval algorithms, which has motivated exploration of machine learning tools (e.g., Segal-Rozenhaimer et al. 2018; Miller et al. 2020). Finally, theoretical studies indicate that MAPs may have the capability to simultaneously retrieve properties of horizontally adjacent aerosol and cloud in a single pixel, given sufficient instrument accuracy (Hasekamp 2010). All of these capabilities, along with efforts to observe cloud and aerosols separately, can provide further insight into ACI.

3D RADIATIVE EFFECTS AS RETRIEVAL ARTIFACTS. In addition to revealing actual changes in near-cloud particle populations, satellite observations also provide insights into the 3D

adjacency effect that influences near-cloud observations from passive instruments. Estimates of contribution of 3D effects to near-cloud enhancements in solar reflectance are shown in Fig. 12 which compares relative enhancements in particle scattering for collocated MODIS and CALIOP observations (Várnai and Marshak 2012). Combining data from the two instruments is instructive, because while MODIS aerosol observations are affected by 3D radiative effects triggered by scattering from nearby clouds (Marshak et al. 2008; Várnai and Marshak 2009), CALIOP observations are not affected the same way since nearby clouds do not contribute to the backscattered signal of the illuminated aerosol column. The scattering contributions of aerosol and undetected cloud particles to the MODIS 555-nm reflectance (R_p) can be obtained by removing the contributions of surface reflection and Rayleigh scattering as estimated for completely aerosol- and cloud-free columns by the MODIS DT algorithm (Levy et al. 2013). In turn, particle contributions to the below-3-km integrated CALIOP 532-nm backscatter (β_p) can be obtained by removing the effects of Rayleigh scattering and ozone absorption.

Figure 12 shows good agreement between CALIOP and MODIS farther than about 10 km from clouds, suggesting a weakening of 3D effects at such distance. But within 5 km from clouds, 3D radiative effects due to cloud adjacency (Marshak et al. 2008) affect MODIS but not CALIOP observations, and appear as a near-cloud enhancement that is 30% larger for MODIS than for CALIOP. Thus, the figure suggests that roughly 30% of near-cloud MODIS enhancements come from 3D effects, while the remaining 70% are due to modified aerosol and cloud particles affecting both CALIOP and MODIS observations and are missed by the MODIS cloud mask used for cloud screening in this study. Note that simulations applying the MODIS instrument point spread functions (Meister and McClain 2010) indicated that instrument blurring plays a modest role beyond 1 km from clouds (Várnai et al. 2013).

Correlation between cloud fraction and aerosol properties

While Figs. 1, 8, and 12 showed the way aerosol properties change with distance to nearest clouds (see also Su et al. 2008; Tackett and Di Girolamo 2009; Redemann et al. 2009), many studies (e.g., Loeb and Manalo-Smith 2005; Zhang et al. 2005) examined how aerosol properties covary with regional CF. Several of these studies rely on instantaneous (“snapshot”) daily gridded cloud and aerosol data resolved at spatial scales ~ 100 km (e.g., Gryspeerdt et al. 2014a) and even examine the CF–aerosol covariation for various types of cloudiness (Oreopoulos et al. 2017; Oreopoulos et al. 2020). Even at these coarse resolutions, efforts have been extended to distinguish cause and effect by rudimentary temporal tracking (Gryspeerdt et al. 2014b) and accounting for meteorological covariations (Gryspeerdt et al. 2016). Figure 13a is an example of a detailed representation of the overwhelmingly positive correlation between the CF of low (liquid) clouds and AOD from MODIS data (Várnai and Marshak 2018) which persists regardless of aerosol type and season and

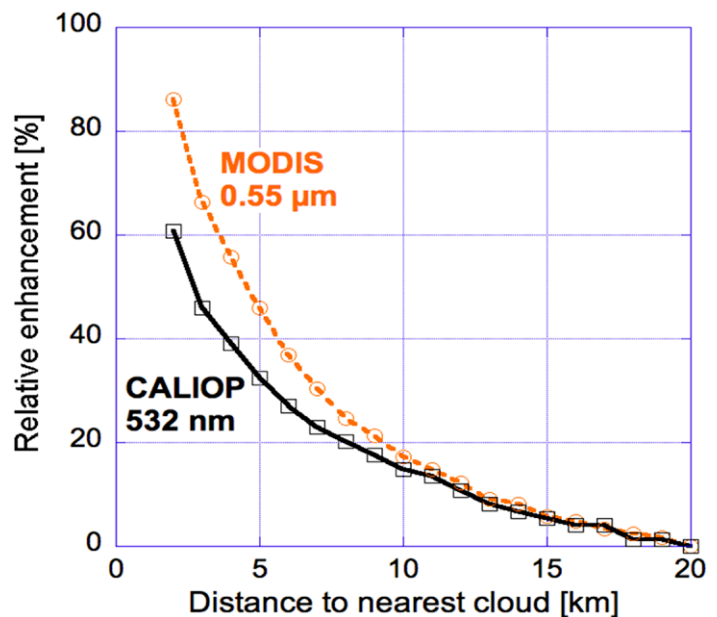


Fig. 12. Median near-cloud relative enhancements in particle scattering, based on MODIS and CALIOP data over all oceans between 60°N and 60°S. Relative enhancements are over the median values 20 km away from clouds. The figure is based on Fig. 4 from Várnai et al. (2013) with permission.

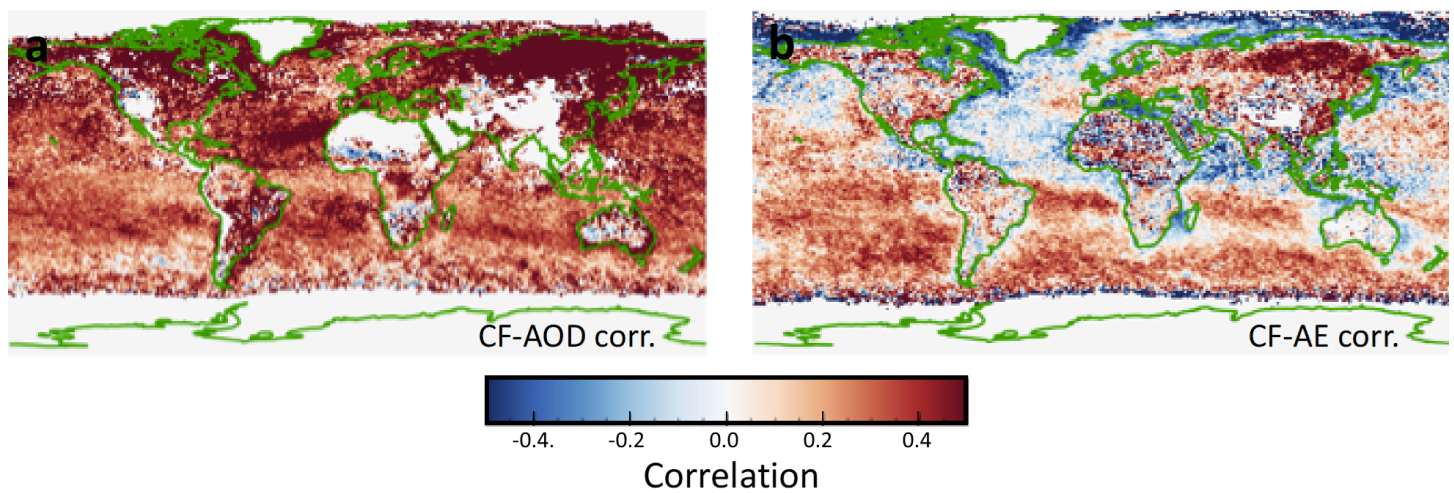


Fig. 13. Maps of correlation between MODIS cloud fraction and (a) aerosol optical depth or (b) Ångström exponent. The local correlation values are shown for each $1^\circ \times 1^\circ$ region, for June–August in 2012–14. Map of the correlation between cloud fraction and Ångström exponent is based the MODIS dark target product over the ocean and the Deep Blue retrieval product over land. The figure is from Várnai and Marshak (2018) with permission.

echoes the findings of the studies employing gridded data and cloud regimes. This persistent CF–AOD relationship has been attributed to factors ranging from cloud lifetime effect to cloud processing and aerosols swelling in the humid air that surrounds clouds. Remote sensing artifacts (especially cloud detection uncertainties and 3D radiative processes), may play a role in the CF–AOD relationship being stronger in satellite datasets (Chand et al. 2012) than in global models (Quaas et al. 2010).

In contrast to the positive CF–AOD correlation, Fig. 13b shows that the correlation between CF and AE can be either positive or negative. A negative correlation is consistent with aerosols swelling in cloudier (thus more humid) days, as decreasing AE values suggest an increasing particle size. However, Fig. 13b also features large regions with positive CF–AE correlations, indicating that in large parts of the planet, higher cloud fraction is associated with smaller aerosol particles. The contrasting behaviors in different regions may be traced back to similar physical processes—for example, aerosol swelling can explain both the negative and the positive CF–AE correlations in Fig. 13b (see also the “Ground-based remote sensing of aerosol–cloud interactions” section and Fig. 4b). This is because in bimodal aerosol populations where swelling impacts coarse mode particles at least as much as it impacts fine mode particles, the overall AE will decrease with increasing CF, indicating a stronger particle size growth in cloudier days. If, however, coarse mode particles are less hygroscopic or occur mainly above the cloud layer, the swelling caused by cloud-related humidity surges in cloudier regions will enhance the radiative impact more for small mode particles than for coarse mode particles, and this will shift the effective particle size of bimodal distributions toward smaller sizes and correspondingly larger AE values (Várnai et al. 2017). To summarize, the negative correlation between CF and aerosol particle size can be explained by (i) fine mode particles swelling more than coarse mode particles (Eck et al. 2014), (ii) cloud processing creating small aerosols (Su et al. 2008; Loeb and Schuster 2008) and, finally, (iii) 3D radiative adjacency effects (Wen et al. 2008). This dual behavior then illustrates that the sign of CF–AE correlation by itself cannot reveal the direction of particle size changes, and that the effect of cloudiness on aerosol size cannot be fully captured by changes in AE alone.

Possible correction of 3D radiative effects near clouds

In passive satellite remote sensing, the reflected solar radiation is used to infer the atmosphere and surface properties in the instrument’s field of view (FOV). While one-dimensional (1D)

radiative transfer models are used operationally to retrieve aerosol properties, the reflectance from clear areas can be significantly affected by 3D radiative effects, namely, enhanced reflectance from nearby clear regions from photons bounced off clouds. Wen et al. (2008) showed that Rayleigh scattering of cloud-reflected sunlight is the dominant mechanism for the reflectance enhancement in the clear areas near clouds. Because of stronger Rayleigh scattering in shorter wavelength, the 3D cloud effects can lead to an apparent “bluing” of clear region (Marshak et al. 2008). Thus, the enhanced radiation creates bias not only in total AOD but also in aerosol size retrievals. Not accounting for cloud 3D effects may cause incorrect interpretation of satellite-based aerosol data near clouds and hence inaccurate quantification of aerosol radiative effects or ACI.

Marshak et al. (2008) showed that the simple two-layer model (2LM) illustrated in Fig. 14 can account for the radiative interactions between boundary layer clouds and clear air above and be used to correct for near-cloud enhancement. The 2LM considers the processes that affect radiation reflected from clouds as it travels through the molecular layer above clouds. These radiative transfer processes include scattering and extinction by air molecules and multiple reflections between the cloud layer and the molecular layer above it. Only solar radiation reflected by clouds and subsequently scattered by the molecular layer above contributes to the cloud-induced enhancement of reflectance).

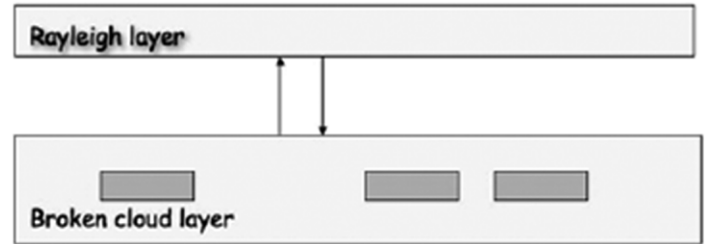


Fig. 14. A schematic two-layer model of a broken cloud field (lower layer) and Rayleigh scatterers (upper layer). Based on Fig. 2 in Marshak et al. (2008) with permission.

For a given upward solar radiative flux from broken cloud layer, one can estimate with a 1D model (e.g., DISORT) the total flux and radiance affected by both scattering and extinction as it traverses the molecular layer and reaches the sensor, as well as the radiation solely due to the extinction by the molecular layer from Beer’s law. Their difference, given by Eq. (1) below, is the radiation scattered by molecules and is an estimate of the additional cloud-induced reflectance (ΔR_m) viewed from satellite, as shown by

$$\Delta R_m(\lambda, \Omega, \Omega_o) = \frac{\alpha_c T_m[\tau_m(\lambda), \Omega_o]}{1 - \alpha_c R_m[\tau_m(\lambda), \Omega_o]} \{ T_{m, \text{diff}}[\tau_m(\lambda), \Omega] - T_{m, \text{beam}}[\tau_m(\lambda), \Omega] \}, \quad (1)$$

where α_c is the cloud albedo; $\tau_m(\lambda)$ is the molecular scattering optical depth above cloud top for wavelength λ ; Ω_o and Ω are solar and viewing directions, respectively; T_m and $T_{m, \text{diff}}$ are the transmittances of the molecular layer for collimated sunlight and the diffuse radiation reflected from the cloud layer, respectively; R_m is the reflectance of the molecular layer for upwelling radiation from the cloud layer; and $T_{m, \text{beam}} = \exp[-\tau_m(\lambda)/\mu]$ is the beam transmittance of the molecular layer for upwelling radiation from the cloud layer at a viewing zenith angle with cosine μ .

The one-layer Poisson model for broken clouds (an example of which is shown in Fig. 15) originally proposed by Titov (1990), generalized by Kassianov (2003) to multilayer broken cloud fields, and validated by Zhuravleva and Marshak (2005), was used in 2LM by Marshak et al. (2008) to calculate the cloud reflectance for broken cloudy regions. The main parameters in the model are surface albedo, cloud fraction, averaged cloud optical depth, cloud aspect ratio (ratio of cloud vertical to horizontal dimensions), and prespecified cloud droplet size distribution single scattering albedo and scattering phase function.

Because sunlight scattered by broken clouds increases the downward diffuse radiative flux in nearby clear areas, it leads to the reflectance enhancement through surface reflection.

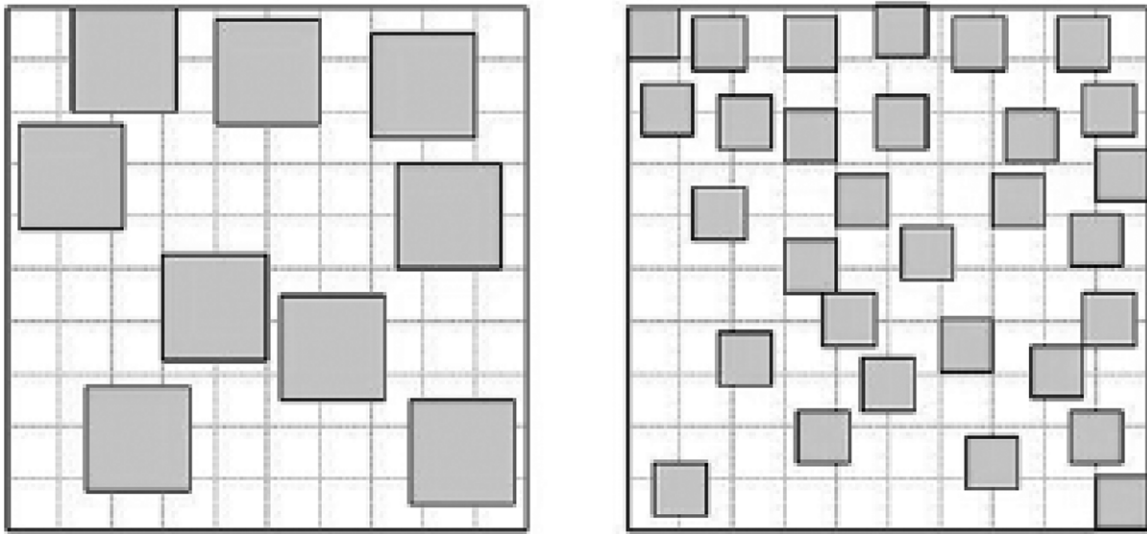


Fig. 15. An example of the Poisson distribution of broken cloud fields with cloud fraction $f_c = 0.3$ for a $10 \text{ km} \times 10 \text{ km}$ area. For a cloud vertical thickness of 1 km, cloud aspect ratio (left) $\gamma=0.5$ and (right) $\gamma=1$. The figure is based on Fig. 4 from Marshak et al. (2008) with permission.

Thus, the reflectance enhancement (ΔR_s) due to cloud-surface radiative interactions can be expressed as

$$\Delta R_s = T_{\text{clear}} \alpha_s e^{-\tau/\mu}, \quad (2)$$

where T_{clear} is the cloud-induced clear area diffuse transmittance (which can be estimated from the Poisson cloud model; Wen et al. 2016), α_s is the surface albedo, and τ is the atmospheric optical depth (aerosol and molecular scattering).

Several scenes were used in Monte Carlo simulations to validate the 2LM (Wen et al. 2007, 2008), before applying the correction model to a full MODIS granule by Wen et al. (2013). These authors corrected for cloud-molecular interactions in the MODIS bands, and the corrected reflectances were then used as inputs in the dark-target MODIS aerosol retrieval algorithm (Remer et al. 2005; Levy et al. 2010). The 2LM model was further tested via comparisons with full 3D radiative transfer simulations on realistic cloud scenes (Wen et al. 2016). The model was found to account for nearly 80% of the cloud-induced reflectance enhancement in nearby clear areas, and is simple enough to be applied as a correction to satellite observations toward inferring the true variation of aerosol near clouds.

Conclusions

This paper discusses aerosol properties in the transition zone between cloudy and clear air, as gleaned from remote sensing observations. The transition zone is a region of strong aerosol-cloud interactions where aerosol particles humidify and swell as they approach the cloud, while cloud droplets evaporate and shrink as they move away from the cloud. The zone consists of fast-changing particle clumps: (i) aerosols at various stages of uptake of water vapor (Loeb and Schuster 2008), (ii) cloud fragments sheared off from neighboring clouds and at various stages of evaporation (Koren et al. 2007), (iii) incipient clouds that are forming but are not yet stable entities (Koren et al. 2009), and (iv) hesitant clouds—pockets of near-saturation humidity that oscillate back and forth from haze to cloud (Feingold and Morley 2003). There is so much of this material that “intercloud region” would be a more appropriate term than “clear.” The intercloud region is a natural laboratory for many phenomena that affect radiation and therefore affect remote sensing signals, but are not yet accounted for in traditional retrievals (Bar-Or et al. 2010).

The IPCC AR5 report clearly states that aerosol properties in the vicinity of clouds are significantly different from those far from clouds. However, retrieval of aerosol properties near clouds from remote sensing observations is quite challenging. Excluding near clouds aerosol dramatically reduces the database and underestimates the forcing, whereas including them may overestimate the forcing. To solve the aerosol–climate problem the transition zone must therefore be directly confronted (Quaas et al. 2010; Chand et al. 2012). When assessing climate model predictions, one must take into account that most passive aerosol retrievals are applied in the high RH environments of nearby clouds. Global datasets of aerosol properties in the vicinity of clouds are currently not available.

In 2018, the U.S. National Academy of Science and Medicine recommended to NASA, NOAA, and the U.S. Geological Survey a decadal strategy for Earth observations from space (National Academies of Sciences, Engineering, and Medicine 2018). In response to this recommendation, NASA is concluding an architecture study for a future mission with transformative measurements of aerosols, clouds, convection and precipitation (ACCP; see <https://aos.gsfc.nasa.gov/>). The study has identified advanced lidars, multiangle polarimeter images, microwave radiometers, and multiwavelength Doppler lidars expected to make substantial contributions to the science of aerosol near cloud discussed in this paper. ACCP will provide the first ever concurrent measurements of vertical resolved cloud and aerosol properties on a global scale, along vertical air motion within clouds.

This overview closely relates to targeted observables of the ACCP mission, as it attempts to interpret apparent aerosol properties near clouds. It surveys the current state of knowledge on aerosol properties near low clouds and discusses the quality of aerosol property observations from existing sensors used from ground, aircraft and satellite vantage points. It summarizes the previously documented correlations between cloudiness and aerosol properties such as AOD and AE. Finally, it demonstrates that 3D radiative effects causing retrieval artifacts near-cloud areas can be simulated, quantified, and corrected. Still, this first comprehensive attempt to review the current state of knowledge on remotely sensed aerosol properties in cloudy environments makes abundantly clear that *to better define aerosol properties near clouds* additional research and high-quality innovative measurements will be required.

Acknowledgments. This study was made possible with support by the Science Task Group program of NASA Goddard Space Flight Center's (GSFC's) Science and Exploration Directorate

References

- Arola, A., T. F. Eck, H. Kokkola, M. R. A. Pitkänen, and S. Romakkaniemi, 2017: Assessment of cloud-related fine-mode AOD enhancements based on AERONET SDA product. *Atmos. Chem. Phys.*, **17**, 5991–6001, <https://doi.org/10.5194/acp-17-5991-2017>.
- Bar-Or, R. Z., I. Koren, and O. Altaratz, 2010: Estimating cloud field coverage using morphological analysis. *Environ. Res. Lett.*, **5**, 014022, <https://doi.org/10.1088/1748-9326/5/1/014022>.
- Chand, D., and Coauthors, 2012: Aerosol optical depth increase in partly cloudy conditions. *J. Geophys. Res.*, **117**, D17207, <https://doi.org/10.1029/2012JD017894>.
- Charlson, R. J., A. S. Ackerman, F. A.-M. Bender, T. L. Anderson, and Z. Liu, 2007: On the climate forcing consequences of the albedo continuum between cloudy and clear air. *Tellus*, **59B**, 715–727, <https://doi.org/10.1111/j.1600-0889.2007.00297.x>.
- Cornet, C., L. C.-Labonnote, and F. Szczap, 2010: Three-dimensional polarized Monte Carlo atmospheric radiative transfer model (3DMCPOL): 3D effects on polarized visible reflectances of a cirrus cloud. *J. Quant. Spectrosc. Radiat. Transfer*, **111**, 174–186, <https://doi.org/10.1016/j.jqsrt.2009.06.013>.
- Dall'Osto, M., R. M. Harrison, H. Coe, and P. Williams, 2009: Real-time secondary aerosol formation during a fog event in London. *Atmos. Chem. Phys.*, **9**, 2459–2469, <https://doi.org/10.5194/acp-9-2459-2009>.
- Dubovik, O., and M. D. King, 2000: A flexible inversion algorithm for the retrieval of aerosol optical properties from Sun and sky radiance measurements. *J. Geophys. Res.*, **105**, 20 673–20 696, <https://doi.org/10.1029/2000JD900282>.
- , and Coauthors, 2006: The application of spheroid models to account for aerosol particle nonsphericity in remote sensing of desert dust. *J. Geophys. Res.*, **111**, D11208, <https://doi.org/10.1029/2005JD006619>.
- Eck, T. F., and Coauthors, 2012: Fog- and cloud-induced aerosol modification observed by the Aerosol Robotic Network (AERONET). *J. Geophys. Res.*, **117**, D07206, <https://doi.org/10.1029/2011JD016839>.
- , and Coauthors, 2014: Observations of rapid aerosol optical depth enhancements in the vicinity of polluted cumulus clouds. *Atmos. Chem. Phys.*, **14**, 11 633–11 656, <https://doi.org/10.5194/acp-14-11633-2014>.
- , and Coauthors, 2018: Observations of the interaction and transport of fine mode aerosols with cloud and/ or fog in Northeast Asia from Aerosol Robotic Network and satellite remote sensing. *J. Geophys. Res. Atmos.*, **123**, 5560–5587, <https://doi.org/10.1029/2018JD028313>.
- , and Coauthors, 2020: Influence of cloud, fog, and high relative humidity during pollution transport events in South Korea: Aerosol properties and PM_{2.5} variability. *Atmos. Environ.*, **232**, 117530, <https://doi.org/10.1016/j.atmosenv.2020.117530>.
- Feingold, G., and B. Morley, 2003: Aerosol hygroscopic properties as measured by lidar and comparison with in situ measurements. *J. Geophys. Res.*, **108**, 4327, <https://doi.org/10.1029/2002JD002842>.
- Flower, V. J. B., and R. A. Kahn, 2020: The evolution of Iceland volcano emissions, as observed from space in the era of NASA's Earth Observing System (EOS). *J. Geophys. Res. Atmos.*, **125**, e2019JD031625, <https://doi.org/10.1029/2019JD031625>.
- Gryspeerdt, E., P. Stier, and B. S. Grandey, 2014a: Cloud fraction mediates the aerosol optical depth-cloud top height relationship. *Geophys. Res. Lett.*, **41**, 3622–3627, <https://doi.org/10.1002/2014GL059524>.
- , —, and D. G. Partridge, 2014b: Satellite observations of cloud regime development: The role of aerosol processes. *Atmos. Chem. Phys.*, **14**, 1141–1158, <https://doi.org/10.5194/acp-14-1141-2014>.
- , J. Quaas, and N. Bellouin, 2016: Constraining the aerosol influence on cloud fraction. *J. Geophys. Res. Atmos.*, **121**, 3566–3583, <https://doi.org/10.1002/2015JD023744>.
- Hasekamp, O. P., 2010: Capability of multi-viewing-angle photo-polarimetric measurements for the simultaneous retrieval of aerosol and cloud properties. *Atmos. Meas. Tech.*, **3**, 839–851, <https://doi.org/10.5194/amt-3-839-2010>.
- , and J. Landgraf, 2005: Retrieval of aerosol properties over the ocean from multispectral single-viewing-angle measurements of intensity and polarization: Retrieval approach, information content, and sensitivity study. *J. Geophys. Res.*, **110**, D20207, <https://doi.org/10.1029/2005JD006212>.
- , P. Litvinov, and A. Butz, 2011: Aerosol properties over the ocean from PARASOL multiangle photopolarimetric measurements. *J. Geophys. Res.*, **116**, D14204, <https://doi.org/10.1029/2010JD015469>.
- , and Coauthors, 2019a: Aerosol measurements by SPeXone on the NASA PACE mission: Expected retrieval capabilities. *J. Quant. Spectrosc. Radiat. Transfer*, **227**, 170–184, <https://doi.org/10.1016/j.jqsrt.2019.02.006>.
- , E. Gryspeerdt, and J. Quaas, 2019b: Analysis of polarimetric satellite measurements suggests stronger cooling due to aerosol-cloud interactions. *Nat. Commun.*, **10**, 5405, <https://doi.org/10.1038/s41467-019-13372-2>.
- Holben, B. N., and Coauthors, 1998: AERONET—A federated instrument network and data archive for aerosol characterization. *Remote Sens. Environ.*, **66**, 1–16, [https://doi.org/10.1016/S0034-4257\(98\)00031-5](https://doi.org/10.1016/S0034-4257(98)00031-5).
- Jethva, H., O. Torres, L. A. Remer, and P. K. Bhartia, 2013: A color ratio method for simultaneous retrieval of aerosol and cloud optical thickness of above-cloud absorbing aerosols from passive sensors: Application to MODIS measurements. *IEEE Trans. Geosci. Remote Sens.*, **99**, 1–9, <https://doi.org/10.1109/TGRS.2012.2230008>.
- , —, F. Waquet, D. Chand, and Y. Hu, 2014: How do A-train sensors intercompare in the retrieval of above-cloud aerosol optical depth? A case study-based assessment. *Geophys. Res. Lett.*, **41**, 186–192, <https://doi.org/10.1002/2013GL058405>.
- Kahn, R. A., and B. J. Gaitley, 2015: An analysis of global aerosol type as retrieved by MISR. *J. Geophys. Res.*, **120**, 4248–4281, <https://doi.org/10.1002/2015JD023322>.
- Kassianov, E., 2003: Stochastic radiative transfer in multilayer broken clouds. Part I: Markovian approach. *J. Quant. Spectrosc. Radiat. Transfer*, **77**, 373–394, [https://doi.org/10.1016/S0022-4073\(02\)00170-X](https://doi.org/10.1016/S0022-4073(02)00170-X).
- Knobelspiesse, K., B. Cairns, J. Redemann, R. W. Bergstrom, and A. Stohl, 2011: Simultaneous retrieval of aerosol and cloud properties during the MILAGRO field campaign. *Atmos. Chem. Phys.*, **11**, 6245–6263, <https://doi.org/10.5194/acp-11-6245-2011>.
- , and Coauthors, 2012: Analysis of fine-mode aerosol retrieval capabilities by different passive remote sensing instrument designs. *Opt. Express*, **20**, 21 457–21 484, <https://doi.org/10.1364/OE.20.021457>.
- , B. Cairns, H. Jethva, M. Kacenelenbogen, M. Segal-Rosenheimer, and O. Torres, 2015: Remote sensing of above cloud aerosols. *Light Scattering Reviews* 9, A. A. Kokhanovsky, Ed., Springer, 167–210.
- Koren, I., L. A. Remer, Y. J. Kaufman, Y. Rudich, and J. V. Martins, 2007: On the twilight zone between clouds and aerosols. *Geophys. Res. Lett.*, **34**, L08805, <https://doi.org/10.1029/2007GL029253>.
- , G. Feingold, H. Jiang, and O. Altaratz, 2009: Aerosol effects on the inter-cloud region of a small cumulus cloud field. *Geophys. Res. Lett.*, **36**, L14805, <https://doi.org/10.1029/2009GL037424>.
- Levy, R. C., L. A. Remer, R. G. Kleidman, S. Mattoo, C. Ichoku, R. Kahn, and T. F. Eck, 2010: Global evaluation of the Collection 5 MODIS dark-target aerosol products over land. *Atmos. Chem. Phys.*, **10**, 10 399–10 420, <https://doi.org/10.5194/acp-10-10399-2010>.
- , S. Mattoo, L. A. Munchak, L. A. Remer, A. M. Sayer, F. Patadia, and N. C. Hsu, 2013: The collection 6 MODIS aerosol products over land and ocean. *Atmos. Meas. Tech.*, **6**, 2989–3034, <https://doi.org/10.5194/amt-6-2989-2013>.
- Li, Z., and Coauthors, 2014: Observations of residual submicron fine aerosol particles related to cloud and fog processing during a major pollution event in Beijing. *Atmos. Environ.*, **86**, 187–192, <https://doi.org/10.1016/j.atmosenv.2013.12.044>.
- , W. Hou, J. Hong, F. Zheng, D. Luo, J. Wang, X. Gu, and Y. Qiao, 2018: Directional Polarimetric Camera (DPC): Monitoring aerosol spectral optical properties over land from satellite observation. *J. Quant. Spectrosc. Radiat. Transfer*, **218**, 21–37, <https://doi.org/10.1016/j.jqsrt.2018.07.003>.
- Limbacher, J. A., and R. A. Kahn, 2019: Updated MISR dark water research aerosol retrieval algorithm—Part 2: Aerosol and surface-reflectance retrievals over

- shallow, turbid, and eutrophic water. *Atmos. Meas. Tech.*, **12**, 675–689, <https://doi.org/10.5194/amt-12-675-2019>.
- Loeb, N. G., and N. Manalo-Smith, 2005: Top-of-atmosphere direct radiative effect of aerosols over global oceans from merged CERES and MODIS observations. *J. Climate*, **18**, 3506–3526, <https://doi.org/10.1175/JCLI3504.1>.
- , and G. L. Schuster, 2008: An observational study of the relationship between cloud, aerosol and meteorology in broken low-level cloud conditions. *J. Geophys. Res.*, **113**, D14214, <https://doi.org/10.1029/2007JD009763>.
- Lyapustin, A., Y. Wang, S. Korkin, and D. Huang, 2018: MODIS Collection 6 MAIAC algorithm. *Atmos. Meas. Tech.*, **11**, 5741–5765, <https://doi.org/10.5194/amt-11-5741-2018>.
- Ma, T., and Coauthors, 2020: Contribution of hydroxymethanesulfonate (HMS) to severe winter haze in the North China Plain. *Atmos. Chem. Phys.*, **20**, 5887–5897, <https://doi.org/10.5194/acp-20-5887-2020>.
- Marshall, A., G. Wen, J. A. Coakley, L. A. Remer, N. G. Loeb, and R. F. Cahalan, 2008: A simple model for the cloud adjacency effect and the apparent blurring of aerosols near clouds. *J. Geophys. Res.*, **113**, D14S17, <https://doi.org/10.1029/2007JD009196>.
- Martins, V. S., A. Lyapustin, Y. Wang, D. M. Giles, A. Smirnov, I. Slutsker, and S. Korkin, 2019: Global validation of columnar water vapor derived from EOS MODIS-MAIAC algorithm against the ground-based AERONET observations. *Atmos. Res.*, **225**, 181–192, <https://doi.org/10.1016/j.atmosres.2019.04.005>.
- Meister, G., and C. R. McClain, 2010: Point-spread function of the ocean color bands of the moderate resolution imaging spectroradiometer on Aqua. *Appl. Opt.*, **49**, 6276–6285, <https://doi.org/10.1364/AO.49.006276>.
- Meyer, K., S. Platnick, and Z. Zhang, 2015: Simultaneously inferring above-cloud absorbing aerosol optical thickness and underlying liquid phase cloud optical and microphysical properties using MODIS. *J. Geophys. Res. Atmos.*, **120**, 5524–5547, <https://doi.org/10.1002/2015JD023128>.
- Miller, D. J., M. Segal-Rozenhaimer, K. Knobelspiesse, J. Redemann, B. Cairns, M. Alexandrov, B. van Dienenhoven, and A. Wasilewski, 2020: Low-level liquid cloud properties during ORACLES retrieved using airborne polarimetric measurements and a neural network algorithm. *Atmos. Meas. Tech.*, **13**, 3447–3470, <https://doi.org/10.5194/amt-13-3447-2020>.
- Mishchenko, M. I., B. Cairns, J. E. Hansen, L. D. Travis, R. Burg, Y. J. Kaufman, J. Vanderlei Martins, and E. P. Shettle, 2004: Monitoring of aerosol forcing of climate from space: Analysis of measurement requirements. *J. Quant. Spectrosc. Radiat. Transfer*, **88**, 149–161, <https://doi.org/10.1016/j.jqsrt.2004.03.030>.
- Moch, J. M., and Coauthors, 2018: Contribution of hydroxymethane sulfonate to ambient particulate matter: A potential explanation for high particulate sulfur during severe winter haze in Beijing. *Geophys. Res. Lett.*, **45**, 11 969–11 979, <https://doi.org/10.1029/2018GL079309>.
- National Academies of Sciences, Engineering, and Medicine, 2018: *Thriving on Our Changing Planet: A Decadal Strategy for Earth Observation from Space*. The National Academies Press, 716 pp., <https://doi.org/10.17226/24938>.
- Nelson, D. L., M. J. Garay, R. A. Kahn, and B. A. Dunst, 2013: Stereoscopic height and wind retrievals for aerosol plumes with the MISR Interactive Explorer (MINX). *Remote Sens.*, **5**, 4593–4628, <https://doi.org/10.3390/rs5094593>.
- Oreopoulos, L., N. Cho, and D. Lee, 2017: Using MODIS cloud regimes to sort diagnostic signals of aerosol-cloud-precipitation interactions. *J. Geophys. Res. Atmos.*, **122**, 5416–5440, <https://doi.org/10.1002/2016JD026120>.
- , ———, and ———, 2020: A global survey of apparent aerosol-cloud interaction signals. *J. Geophys. Res. Atmos.*, **125**, e2019JD031287, <https://doi.org/10.1029/2019JD031287>.
- Parol, F., and Coauthors, 2004: Review of capabilities of multi-angle and polarization cloud measurements from POLDER. *Adv. Space Res.*, **33**, 1080–1088, [https://doi.org/10.1016/S0273-1177\(03\)00734-8](https://doi.org/10.1016/S0273-1177(03)00734-8).
- Peers, F., and Coauthors, 2015: Absorption of aerosols above clouds from POLDER/ PARASOL measurements and estimation of their direct radiative effect. *Atmos. Chem. Phys.*, **15**, 4179–4196, <https://doi.org/10.5194/acp-15-4179-2015>.
- Quaas, J., B. Stevens, P. Stier, and U. Lohmann, 2010: Interpreting the cloud cover—Aerosol optical depth relationship found in satellite data using a general circulation model. *Atmos. Chem. Phys.*, **10**, 6129–6135, <https://doi.org/10.5194/acp-10-6129-2010>.
- Redemann, J., Q. Zhang, P. B. Russell, J. M. Livingston, and L. A. Remer, 2009: Case studies of aerosol remote sensing in the vicinity of clouds. *J. Geophys. Res.*, **114**, D06209, <https://doi.org/10.1029/2008JD010774>.
- Remer, L. A., and Coauthors, 2005: The MODIS aerosol algorithm, products, and validation. *J. Atmos. Sci.*, **62**, 947–973, <https://doi.org/10.1175/JAS3385.1>.
- , and Coauthors, 2019: Retrieving aerosol characteristics from the PACE mission, Part 2: Multi-angle and polarimetry. *Front. Environ. Sci.*, **7**, 94, <https://doi.org/10.3389/fenvs.2019.00094>.
- Sayer, A. M., N. C. Hsu, C. Bettenhausen, J. Lee, J. Redemann, B. Schmid, and Y. Shinzuka, 2016: Extending “Deep Blue” aerosol retrieval coverage to cases of absorbing aerosols above clouds: Sensitivity analysis and first case studies. *J. Geophys. Res. Atmos.*, **121**, 4830–4854, <https://doi.org/10.1002/2015JD024729>.
- Segal-Rozenhaimer, M., D. J. Miller, K. Knobelspiesse, J. Redemann, B. Cairns, and M. D. Alexandrov, 2018: Development of neural network retrievals of liquid cloud properties from multi-angle polarimetric observations. *J. Quant. Spectrosc. Radiat. Transfer*, **220**, 39–51, <https://doi.org/10.1016/j.jqsrt.2018.08.030>.
- Spencer, R. S., and Coauthors, 2019: Exploring aerosols near clouds with high-spatial-resolution aircraft remote sensing during SEAC⁴RS. *J. Geophys. Res. Atmos.*, **124**, 2148–2173, <https://doi.org/10.1029/2018JD028989>.
- Stap, F., O. Hasekamp, and T. Roekmann, 2015: Sensitivity of PARASOL multi-angle photopolarimetric aerosol retrievals to cloud contamination. *Atmos. Meas. Tech.*, **8**, 1287–1301, <https://doi.org/10.5194/amt-8-1287-2015>.
- , ———, C. Emde, and T. Röckmann, 2016: Multiangle photopolarimetric aerosol retrievals in the vicinity of clouds: Synthetic study based on a large eddy simulation. *J. Geophys. Res. Atmos.*, **121**, 12 914–12 935, <https://doi.org/10.1002/2016JD024787>.
- Su, W., G. L. Schuster, N. G. Loeb, R. R. Rogers, R. A. Ferrare, C. A. Hostetler, J. W. Hair, and M. D. Obland, 2008: Aerosol and cloud interaction observed from high spectral resolution lidar data. *J. Geophys. Res.*, **113**, D24202, <https://doi.org/10.1029/2008JD010588>.
- Tackett, J. L., and L. Di Girolamo, 2009: Enhanced aerosol backscatter adjacent to tropical trade wind clouds revealed by satellite-based lidar. *Geophys. Res. Lett.*, **36**, L14804, <https://doi.org/10.1029/2009GL039264>.
- Tanré, D., and Coauthors, 2011: Remote sensing of aerosols by using polarized, directional and spectral measurements within the A-Train: The PARASOL mission. *Atmos. Meas. Tech.*, **4**, 1383–1395, <https://doi.org/10.5194/amt-4-1383-2011>.
- Titov, G. A., 1990: Statistical description of radiation transfer in clouds. *J. Atmos. Sci.*, **47**, 24–38, [https://doi.org/10.1175/1520-0469\(1990\)047<0024:SDORTI>2.0.CO;2](https://doi.org/10.1175/1520-0469(1990)047<0024:SDORTI>2.0.CO;2).
- Twohy, C. H., J. A. Coakley Jr., and W. R. Tahnk, 2009: Effect of changes in relative humidity on aerosol scattering near clouds. *J. Geophys. Res.*, **114**, D05205, <https://doi.org/10.1029/2008JD010991>.
- Várnai, T., and A. Marshall, 2009: MODIS observations of enhanced clear sky reflectance near clouds. *Geophys. Res. Lett.*, **36**, L06807, <https://doi.org/10.1029/2008GL037089>.
- , and ———, 2011: Global CALIPSO observations of aerosol changes near clouds. *IEEE Geosci. Remote Sens. Lett.*, **8**, 19–23, <https://doi.org/10.1109/LGRS.2010.2049982>.
- , and ———, 2012: Analysis of co-located MODIS and CALIPSO observations near clouds. *Atmos. Meas. Tech.*, **5**, 389–396, <https://doi.org/10.5194/amt-5-389-2012>.
- , and ———, 2018: Satellite observations of cloud-related variations in aerosol properties. *Atmosphere*, **9**, 430, <https://doi.org/10.3390/atmos9110430>.
- , ———, and W. Yang, 2013: Multi-satellite aerosol observations in the vicinity of clouds. *Atmos. Chem. Phys.*, **13**, 3899–3908, <https://doi.org/10.5194/acp-13-3899-2013>.

- , ——, and T. F. Eck, 2017: Observation-based study on aerosol optical depth and particle size in partly cloudy regions. *J. Geophys. Res. Atmos.*, **122**, 102013–102024, <https://doi.org/10.1002/2017JD027028>.
- Waquet, F., J. Riedi, L. Labonnote, P. Goloub, B. Cairns, J. L. Deuzé, and D. Tanré, 2009: Aerosol remote sensing over clouds using A-Train observations. *J. Atmos. Sci.*, **66**, 2468–2480, <https://doi.org/10.1175/2009JAS3026.1>.
- , and Coauthors, 2013: Retrieval of aerosol microphysical and optical properties above liquid clouds from POLDER/PARASOL polarization measurements. *Atmos. Meas. Tech.*, **6**, 991–1016, <https://doi.org/10.5194/amt-6-991-2013>.
- Wen, G., A. Marshak, R. F. Cahalan, L. Remer, and R. G. Kleidman, 2007: 3D aerosol-cloud radiative interaction observed in collocated MODIS and ASTER images of cumulus cloud fields. *J. Geophys. Res.*, **112**, D13204, <https://doi.org/10.1029/2006JD008267>.
- , ——, and ——, 2008: Importance of molecular Rayleigh scattering in the enhancement of clear sky radiance in the vicinity of boundary layer cumulus clouds. *J. Geophys. Res.*, **113**, D24207, <https://doi.org/10.1029/2008JD010592>.
- , ——, L. Remer, R. Levy, N. Loeb, T. Várnai, and R. Cahalan, 2013: Correction of MODIS aerosol retrieval for 3D radiative effects in broken cloud fields. *AIP Conf. Proc.*, **1531**, 280, <https://doi.org/10.1063/1.4804761>.
- , ——, T. Várnai, and R. C. Levy, 2016: Testing the two-layer model for correcting near cloud reflectance enhancement using LES/SHDOM simulated radiances. *J. Geophys. Res. Atmos.*, **121**, 9661–9674, <https://doi.org/10.1002/2016JD025021>.
- Winker, D. M., M. A. Vaughan, A. Omar, Y. Hu, K. A. Powell, Z. Liu, W. H. Hunt, and S. A. Young, 2007: Overview of the CALIPSO mission and CALIOP data processing algorithms. *J. Atmos. Oceanic Technol.*, **26**, 2310–2323, <https://doi.org/10.1175/2009JTECHA1281.1>.
- Xu, F., and Coauthors, 2018: Coupled retrieval of liquid water cloud and above-Cloud aerosol properties using the Airborne Multiangle SpectroPolarimetric Imager (AirMSPI). *J. Geophys. Res. Atmos.*, **123**, 3175–3204, <https://doi.org/10.1002/2017JD027926>.
- Yang, W., A. Marshak, T. Várnai, O. V. Kalashnikova, and A. B. Kostinski, 2012: CALIPSO observations of transatlantic dust properties: vertical stratification and effect of clouds. *Atmos. Chem. Phys.*, **12**, 11 339–11 354, <https://doi.org/10.5194/acp-12-11339-2012>.
- Yu, H., and Z. Zhang, 2013: New directions: Emerging satellite observations of above-cloud aerosols and direct radiative forcing. *Atmos. Environ.*, **72**, 36–40, <https://doi.org/10.1016/j.atmosenv.2013.02.017>.
- Zhang, J., J. S. Reid, and B. N. Holben, 2005: An analysis of potential cloud artifacts in MODIS over ocean aerosol optical thickness products. *Geophys. Res. Lett.*, **32**, L15803, <https://doi.org/10.1029/2005GL023254>.
- Zhuravleva, T., and A. Marshak, 2005: On the validation of the Poisson model of broken clouds. *Izv., Atmos. Ocean. Phys.*, **41**, 713–725.